



OPEN

Thermodynamic insight into the growth of nanoscale inclusion of Al-deoxidation in Fe–O–Al melt

Hong Lei¹, Yuanyou Xiao², Guocheng Wang^{2✉}, Hongwei Zhang¹, Wei Jin³ & Lifeng Zhang⁴

Products of Al-deoxidation reaction in iron melt are the most common inclusions and play an important effect on steel performance. Understanding the thermodynamics on nano-alumina (or nano-hercynite) is very critical to explore the relationship between Al-deoxidation reaction and products growth in iron melt. In present study, a thermodynamic modeling of nano-alumina inclusions in Fe–O–Al melt has been developed. The thermodynamic results show that the Gibbs free energy changes for the formation of nano- Al_2O_3 and nano- FeAl_2O_4 decrease with the increasing size and increase with the increasing temperature. The Gibbs free energy changes for transformation of nano- Al_2O_3 into bulk- Al_2O_3 increase with the increasing size and temperature. The thermodynamic curve of nano-alumina (or nano-hercynite) and the equilibrium curve of bulk-alumina (or bulk-hercynite) obtained in this work are agree with the published experimental data of Al-deoxidation equilibria in liquid iron. In addition, the thermodynamic coexisting points about Al_2O_3 and FeAl_2O_4 in liquid iron are in a straight line and coincide with the various previous data. It suggested that these scattered experimental data maybe in the different thermodynamic state of Al-deoxidized liquid iron and the reaction products for most of the previous Al-deoxidation experiments are nano-alumina (or nano-hercynite).

Alumina inclusions are harmful to the quality of the steel production, because of their high melting point and high hardness. In order to reduce and eliminate the harm of alumina inclusions, the steelmakers try their best to remove all inclusions, or transform the solid alumina to liquid (or partially liquid) calcium aluminates by Ca treatment^{1,2}. On the other hand, they want to make full use of some special inclusions to improve the steel performance^{3–6}. For example, the fine inclusions can be utilized as nucleation sites and make positive contribution to the nucleation of acicular ferrite^{3–6}. From this point of view, refining of alumina inclusions can be one of the important way to enhance the quality of steel products. To refine the size of alumina inclusions, it is necessary to study the formation process of alumina and the thermodynamics on nanoscale inclusion during Al-deoxidation in molten steel.

In order to investigate the evolution process of alumina inclusion in liquid iron, several researchers^{7–9} carried out their experiments of Al-deoxidation in iron melt by ultra-rapid cooling method. Zhao et al.⁷ carried out the Al-deoxidation experiments in Fe–O melt by ultra-rapid cooling methods and found the shapes of alumina inclusions are small and irregular in various experimental samples. They reported that the equivalent radius of alumina inclusions are between 15 and 150 nm⁷. Wasai et al.⁸ also found a series of small alumina from nanoscale to microscale in Al-deoxidation experiments by this methods. It can be suggested that nano-alumina is the intermediate product of the crystallization of bulk alumina inclusions during Al-deoxidation process. Thus, the thermodynamics of nano-alumina in liquid iron is the basic to investigate the relationship of the size of alumina inclusions and Al-deoxidation reaction. Thermodynamic for Al-deoxidation in liquid iron

¹Key Laboratory of Electromagnetic Processing of Materials, Ministry of Education, Northeastern University, Shenyang 110819, Liaoning Province, P. R. China. ²Key Laboratory of Chemical Metallurgy Engineering Liaoning Province, University of Science and Technology Liaoning, Anshan 114051, Liaoning, P. R. China. ³Key Laboratory of Synthetic and Biological Colloids, Ministry of Education, School of Chemical and Material Engineering, Jiangnan University, Wuxi 214122, Jiangsu Province, P. R. China. ⁴College of Materials Science and Engineering, Yanshan University, Qinhuangdao 066004, Hebei, P. R. China. ✉email: wang_guocheng@163.com

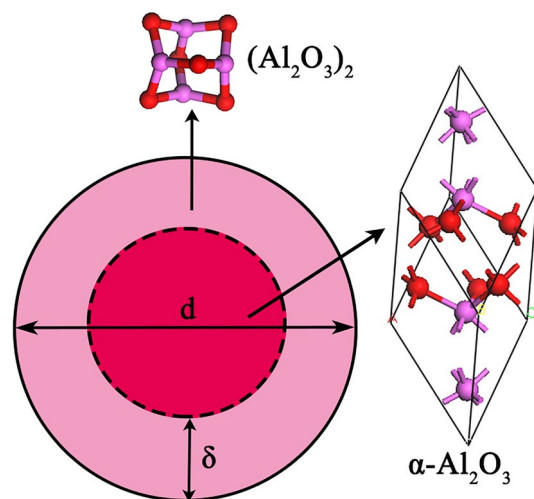


Figure 1. Structure of nano- Al_2O_3 .

have been extensively studied since the middle of twentieth century^{10–30}. However, most of the researchers are focused on the thermodynamic equilibrium between the bulk-alumina and iron melt, while less known about the thermodynamic properties of nano-alumina in liquid iron. Many previous work proved that the thermodynamic properties of the nano-alumina are different from that of the bulk-alumina, and the thermodynamic difference among the nanoscale inclusions is more obvious with the decreasing size of inclusions^{31–38}. It was reported that the interfacial free energy between nano-alumina and liquid iron are decreased with the decreasing of the size of alumina, and the Gibbs free energy change of Al-deoxidation reaction has very close relation with the size change of alumina inclusion³¹. Wang et al.^{32–34} also reported that the thermodynamics of Al-deoxidation reaction in liquid iron is dependent on the size of alumina inclusions. Therefore, a thermodynamic modeling about nano-alumina in liquid iron is necessary.

In this paper, the thermodynamic modeling for Al-deoxidation reaction between nano-alumina inclusions and liquid iron has been developed. Base on the density functional theory (DFT) calculations, the thermodynamic curves and coexisting points corresponding to various size alumina and hercynite inclusions in liquid iron have been obtained. The effect of products size on Al-deoxidation equilibrium thermodynamics have been discussed.

Theoretical calculation

Thermodynamic modeling of nano- Al_2O_3 in Fe–O–Al melt. The nano- Al_2O_3 consists of two parts^{38,39}, an internal part that the atoms located in the lattice of Al_2O_3 crystal and an external part that the atoms situated in the surface layer of Al_2O_3 particle. Thus, the calculations of thermodynamic properties of nano- Al_2O_3 should be dealt with separately. The total Gibbs free energy of nano- Al_2O_3 G can be obtained as^{38,39}

$$G = (1 - x_s)G_i + x_sG_s \quad (1)$$

where G_s and G_i are the Gibbs free energy of the external part and internal part of nano- Al_2O_3 , x_s is the atomic fractions in the surface of nano- Al_2O_3 . As shown in Fig. 1, the nano- Al_2O_3 described as a sphere particle with diameter d , contains a shell of δ thickness and a core with diameter $(d - 2\delta)$. The atomic fractions x_s in the surface of nano- Al_2O_3 can be obtained as

$$x_s = \frac{N_s}{N_s + N_i} = \frac{V_s \rho_s}{V_i \rho_i + V_s \rho_s} = \frac{1 - \left(1 - \frac{2\delta}{d}\right)^3}{1 + \left(\frac{\rho_i}{\rho_s} - 1\right) \left(1 - \frac{2\delta}{d}\right)^3} \quad (2)$$

where the subscripts i and s stand for the internal part or the surface part of nano- Al_2O_3 , N is the atom numbers, V is the volumes, ρ is the atomic densities.

Some experiments reported that the atomic density of nano-particle surface is lower than that of the perfect crystal by 10–30%^{39,40}. Thus, the value of ρ_i/ρ_s was taken as 1.2 in the present calculation. It was reported that the nanocrystalline surface is short-range order structure and there exist a liquid-like structure layer on the surface of nano-particle^{41–43}. As can be seen from Fig. 2, nano- Al_2O_3 is the intermediate of Al_2O_3 product particle growth in the Al-deoxidation reaction, and its surface is formed by the aggregation and phase transformation of $(\text{Al}_2\text{O}_3)_n$ clusters. Therefore, it is logical to conclude that the surface structure of the nano- Al_2O_3 is a short-range order structure and is similar to the structure of $(\text{Al}_2\text{O}_3)_n$ clusters. Furthermore, some studies reported that the surface of nano-particle usually contains two or three atom layers^{5,44}. In this work, for simplicity, the $(\text{Al}_2\text{O}_3)_2$ cluster, which contains three-atom thick, was used to describe the surface structure of nano- Al_2O_3 , and the $\alpha\text{-Al}_2\text{O}_3$ crystal was used to describe the internal part structure of nano- Al_2O_3 as show in Fig. 1. Thus, the Gibbs free

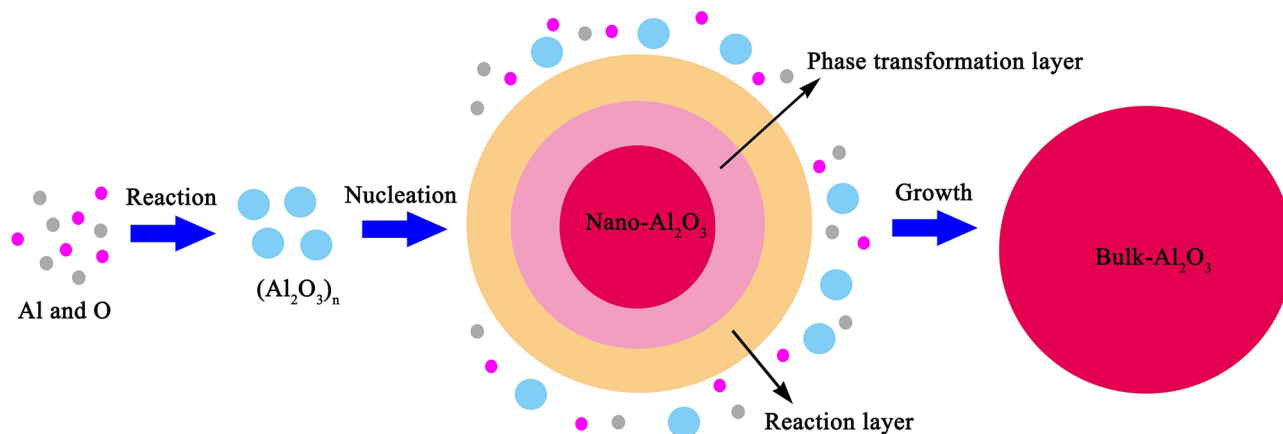


Figure 2. Schematic of the nucleation and growth of Al_2O_3 inclusion.

d (nm)	2	3	4	5	6	8
x_s (%)	85.37	66.43	53.31	44.27	37.76	29.11
d (nm)	10	20	40	60	100	200
x_s (%)	23.65	12.17	6.17	4.13	2.49	1.25

Table 1. Atomic fractions of the surface components.

energy of the internal part of nano- Al_2O_3 equal to the Gibbs free energy of α - Al_2O_3 crystal, and the Gibbs free energy of the external part of nano- Al_2O_3 equal to the Gibbs free energy of $(1/2) (\text{Al}_2\text{O}_3)_2$. Moreover, the length of Al–O bond for alumina cluster is about 0.17 nm^{34} . In other words, the thickness of three atom layers is about 0.5 nm . In this work, the thickness of the nano- Al_2O_3 surface δ was taken as 0.5 nm in calculation. The atomic fraction of the shell components are shown in Table 1.

Calculation methods. The Gibbs free energy of Al_2O_3 clusters and α - Al_2O_3 crystal were calculated by DFT method. During the calculations, the generalized-gradient approximation of Perdew–Burke–Ernzerhof (PBE) was applied as the exchange–correlation potential function⁴⁶. The initial structures of $(\text{Al}_2\text{O}_3)_2$ cluster and α - Al_2O_3 crystal were selected from the previous work³³. The Gibbs free energy of $(\text{Al}_2\text{O}_3)_2$ cluster and α - Al_2O_3 crystal were calculated by the equations^{33–37}

$$G = E + H - TS \quad (3)$$

where E is the total energy of alumina cluster or crystal at 0 K ; H and S are the enthalpy and entropy of alumina cluster or crystal, respectively. The H and S were obtained by the analysis of atomic harmonic vibrational frequency of alumina cluster or crystal, which are the functions of temperature T . The calculation details of the relationship among the atomic harmonic vibrational frequency, the thermodynamic properties and temperature can be found in our previous study^{33–37}.

Gibbs free energy changes for the formation of nano- Al_2O_3 in liquid iron. The reaction equation of Al-deoxidation in Fe–O–Al melt can be written as:



Nano-alumina is the intermediate product of the formation of bulk alumina inclusion and can be formed at first during Al-deoxidation process. The formation of nano- Al_2O_3 in liquid iron can be described as



Then, nano- Al_2O_3 continue to grow up into stable bulk α - Al_2O_3 inclusions, and expressed as



The Gibbs free energy change of the formation of nano- Al_2O_3 as Eq. (5) is ΔG_F^θ , and the Gibbs free energy change for the transformation of nano- Al_2O_3 into bulk- Al_2O_3 as Eq. (6) is ΔG_T^θ . Based on Eqs. (4)–(6), ΔG_F^θ and ΔG_T^θ for the formation and transformation of different size nano- Al_2O_3 in iron melt can be calculated as

$$\Delta G_F^\theta = \Delta G_{\text{Al}_2\text{O}_3(\text{bulk})}^\theta - \Delta G_T^\theta \quad (7)$$

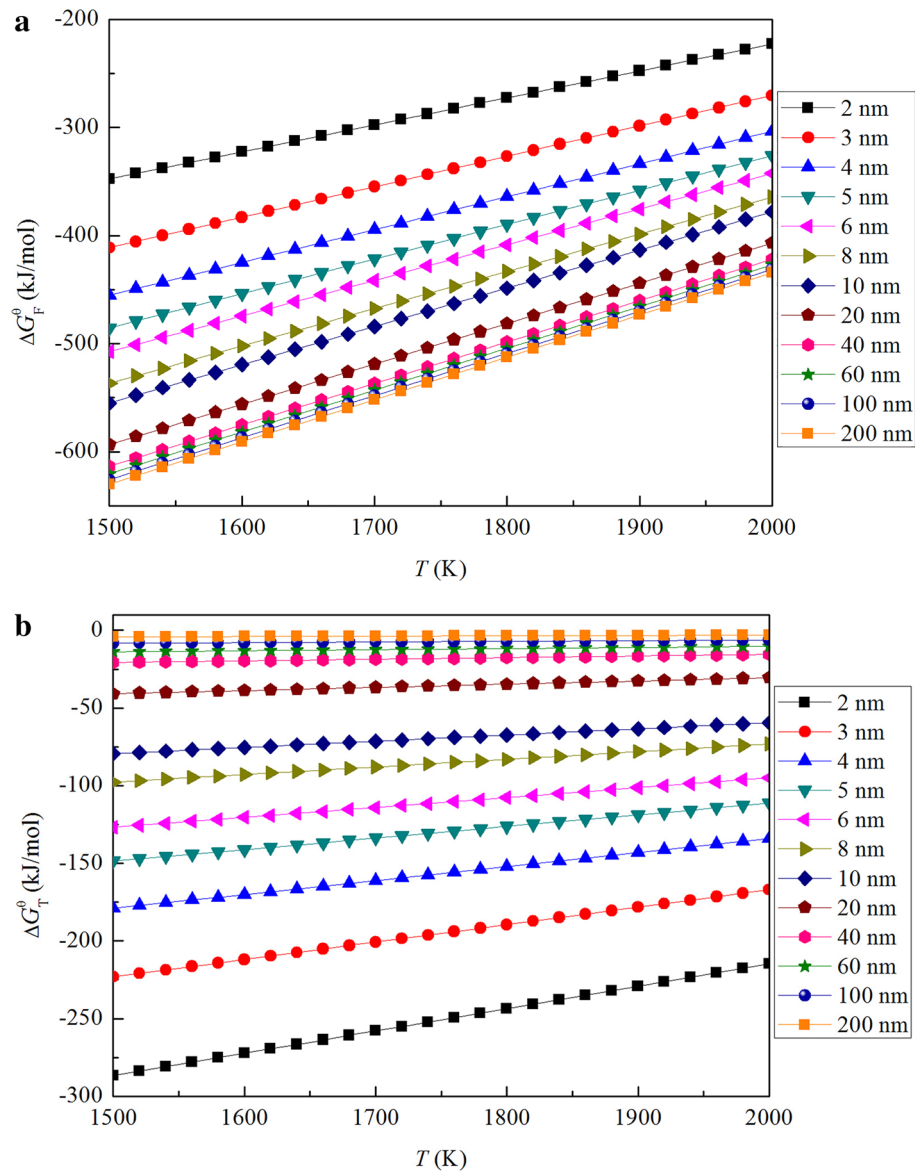


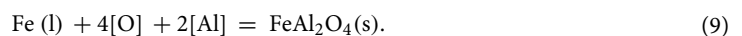
Figure 3. Gibbs free energy changes for the formation and transformation of nano-Al₂O₃ in liquid iron at 1873 K. (a) ΔG_F^θ , (b) ΔG_T^θ .

$$\Delta G_T^\theta = G_{Al_2O_3(bulk)} - G_{nano-Al_2O_3} \quad (8)$$

where $\Delta G_{Al_2O_3(bulk)}^\theta$ is Gibbs free energy change of the formation of α -Al₂O₃(bulk) as Eq. (4), $G_{Al_2O_3(bulk)}$ is Gibbs free energy of α -Al₂O₃ (bulk), $G_{nano-Al_2O_3}$ is Gibbs free energy of nano-Al₂O₃. The value of $\Delta G_{Al_2O_3(bulk)}^\theta$ recommended by JPSP¹⁰ was used in the calculations as: $\Delta G_{Al_2O_3(s)}^\theta = -1,225,000 + 393.8 T$ J/mol.

Figure 3 show the value of ΔG_F^θ and ΔG_T^θ (from 1500 to 2000 K). It can be seen from Fig. 3, ΔG_F^θ decreases with the increasing size of nano-Al₂O₃, while ΔG_T^θ increases with the increasing size of nano-Al₂O₃. It implies that the thermodynamic driving energy for the formation of nano-Al₂O₃ increases gradually with the increasing of alumina size, while the thermodynamic driving energy for transformation of nano-Al₂O₃ into bulk-Al₂O₃ decreases gradually with the increasing of alumina size. On the other hand, the value of ΔG_F^θ and ΔG_T^θ increase with the increasing temperature. This result indicates that both the formation of nano-Al₂O₃ and the transformation of nano-Al₂O₃ into bulk-Al₂O₃ at the low temperature is more easier than that at the high temperature.

Gibbs free energy changes for the formation of nano-FeAl₂O₄ in liquid iron. Hercynite (FeAl₂O₄) is one of the product of Al-deoxidation reaction in liquid iron when [Al] at low content and [O] at high content. The equilibrium between FeAl₂O₄ and Fe–O–Al melt can be expressed as



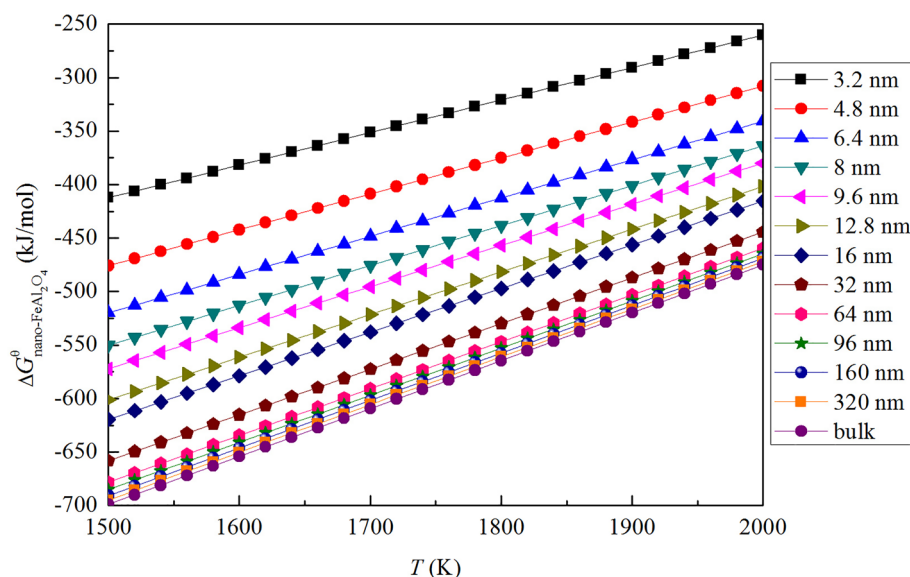
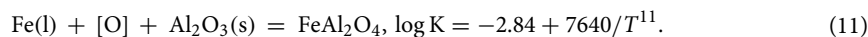


Figure 4. Gibbs free energy changes for the formation nano-FeAl₂O₄ in liquid iron.

The activity of Fe(l) and FeAl₂O₄(s) is unity, and the activity of oxygen and aluminum is approximately its weight percent concentration because of [% Al] < 0.1 and [% O] < 0.1 in the liquid iron. Thus, the equilibrium constant $K_{FeAl_2O_4}$ for Eq. (10) can be expressed as follows

$$\ln K_{FeAl_2O_4} = -\frac{\Delta G_{FeAl_2O_4}^\theta}{RT} = -4 \ln \alpha_{[O]} - 2 \ln \alpha_{[Al]} = -4 \ln[\%O] - 2 \ln[\%Al] \quad (10)$$

where α_i are the activity of element Al and O in the liquid iron, $\Delta G_{FeAl_2O_4}^\theta$ is Gibbs free energy changes for the formation of FeAl₂O₄ in liquid iron and can be calculate by Eqs. (4) and (11)



Nano-FeAl₂O₄ is the intermediate product of the formation of bulk FeAl₂O₄ inclusion during Al-deoxidation process, and the formation of nano-FeAl₂O₄ can be described as



Thus, the Gibbs free energy change for the formation of nano-FeAl₂O₄ in liquid iron $\Delta G_{nano-FeAl_2O_4}^\theta$ can be calculated by Eqs. (5), (11) and (12). The Gibbs free energy changes for the formation of nano-FeAl₂O₄ in liquid iron are shown in Fig. 4. $\Delta G_{nano-FeAl_2O_4}^\theta$ decreases with the increasing size and increases with the increasing temperature. This result implies that the thermodynamic driving energy for the formation of nano-FeAl₂O₄ increases gradually with the increasing of size and decreasing of temperature.

Discussion

Effect of products size on Al-deoxidation equilibrium thermodynamics. The equilibria for Al-deoxidation in liquid iron have been extensively investigated^{12–25}. Table 2 lists the experimental conditions and methods of Al-deoxidation equilibrium in liquid iron at 1873 K. Most of the Al-deoxidation equilibria were measured by equilibrating liquid iron with [Al] and pure solid Al₂O₃ at 1873 K^{12–14,18,19,22–25}. The Al-deoxidation experiments were generally carried out in alumina crucible by using rotating furnace¹², resistance furnace^{19,22} and induction furnace^{23–25}. Equilibrium concentration of [O] and [Al] were determined by analyzing the composition of experimental sample. The concentration of oxygen was generally analyzed by vacuum fusion method^{12,13,18}, inert gas fusion method^{14,19,22–25}, and neutron activation method¹⁵, while that of aluminum was obtained by wet-chemical analysis. On the other hand, in order to make the Al-deoxidation reaction more close to the final equilibrium state in liquid iron, Rohde et al.¹⁶, Suito et al.¹⁹, Paek et al.²⁵ carried out their experiments with covered CaO–Al₂O₃ flux on the liquid iron. Meanwhile, the equilibrium oxygen potential in liquid iron was sometimes directly measured by using Electro Motive Force (EMF) technique^{15,17,20,21}. It can be seen from Fig. 5a that the concentration of [O] decreases with the increasing [Al] when the concentration of [% Al] < 1%. It should be noted that, however, the difference among the concentrations of [O] reported by different researchers at the same concentration of [Al] is close to two order of magnitude.

In order to investigated the thermodynamic equilibrium rule of the Al-deoxidation reaction, most of the researchers^{10,22,24,26–28} established thermodynamic equilibrium curves based on the Wagner's interaction parameter formalism. The thermodynamic equilibria curves obtained by various researchers are plotted as lines in Fig. 5a. At the concentration of [Al] < 0.1%, most of the equilibrium curves agree with their own experiments data and have the same trend that the concentration of [O] decreased with the increasing [Al]. When the [Al]

Authors	Experimental methods	[% Al]	Year
Hilty et al. ¹²	Fe(l)-Al ₂ O ₃ (s)/V, rotating furnace	0.001–0.82	1950
Novokhatski et al. ¹³	Fe(l)-Al ₂ O ₃ (s)/V	0.007–3.9	1966
Schenck et al. ¹⁴	Fe(l)-Al ₂ O ₃ (s)/I	0.02–8.2	1970
Fruehan ¹⁵	EMF/N	0.02–1.4	1970
Rohde et al. ¹⁶	Fe(l)-CaO-Al ₂ O ₃ slag	0.01–2.5	1971
Janke et al. ¹⁷	EMF	0.0003–1.3	1976
Shevtsov et al. ¹⁸	Fe(l)-Al ₂ O ₃ (s)/V	0.01–100	1981
Suito et al. ¹⁹	Fe(l)-CaO-Al ₂ O ₃ slag, Fe(l)-Al ₂ O ₃ (s)/I, resistance furnace	0.001–32.7	1991
Suito, Inoue, Nagatani ²⁰	EMF	0.0006–1.0	1992
Dimitrov et al. ²¹	EMF	0.0001–1.2	1995
Seo et al. ²²	Fe(l)-Al ₂ O ₃ (s)/I, resistance furnace	0.0002–1.0	1998
Hanyashi et al. ²³	Fe(l)-Al ₂ O ₃ (s)/I, induction furnace	0.00031–0.0303	2008
Kang et al. ²⁴	Fe(l)-Al ₂ O ₃ (s)/I, induction furnace	0.01–10	2009
Paek et al. ²⁵	Fe(l)-CaO-Al ₂ O ₃ slag, Fe(l)-Al ₂ O ₃ (s)/I, induction furnace	0.0027–100	2015

Table 2. Experimental conditions and methods for Al-deoxidation equilibrium in liquid iron at 1873 K. *V* vacuum fusion method, *N* neutron activation method, *I* inert gas fusion-infrared absorptiometry method.

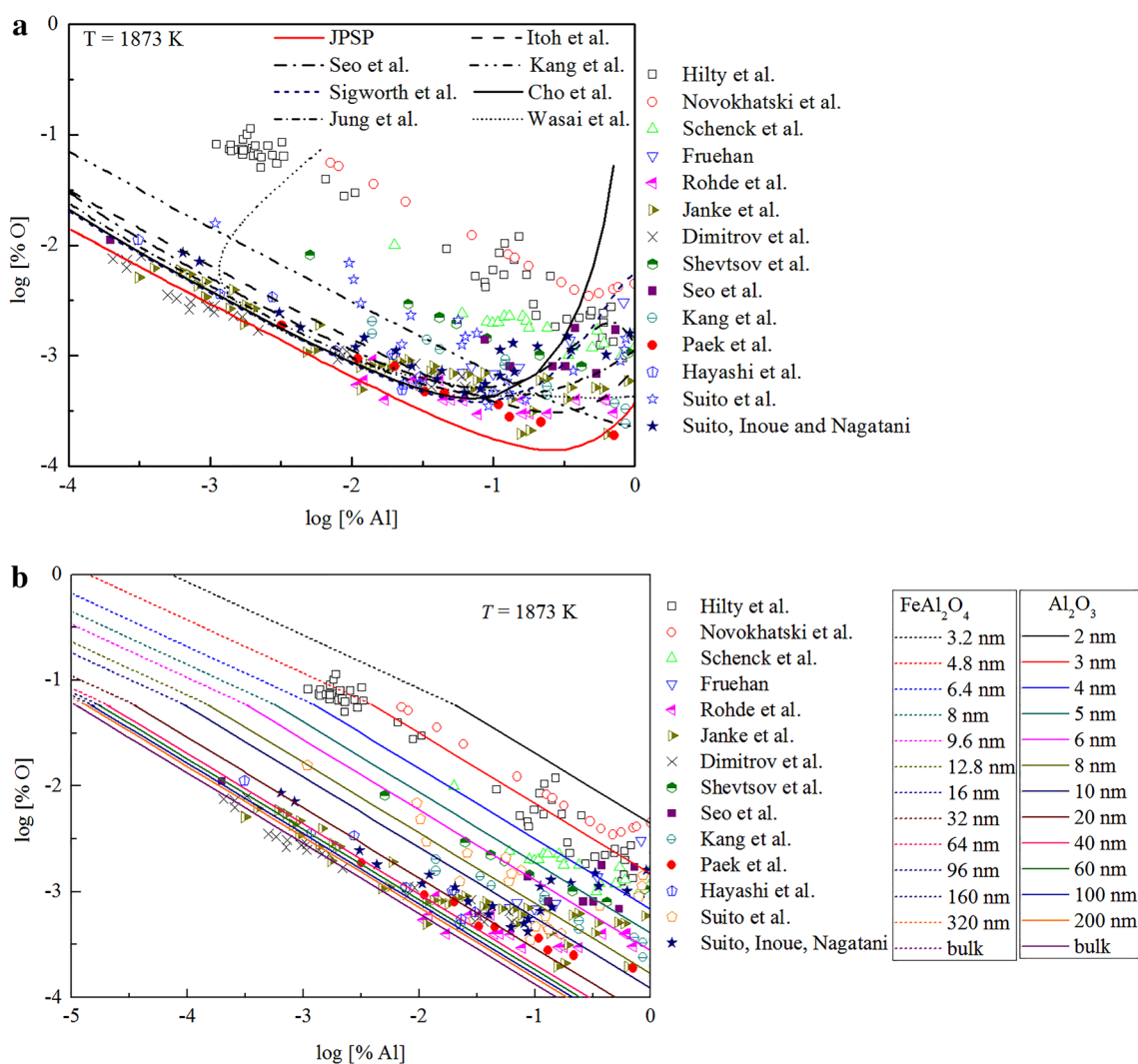


Figure 5. Thermodynamic curves of Al-deoxidation in liquid iron at 1873 K. (a) Equilibrium data obtained by previous work, (b) thermodynamic curves obtained by this work.

content is greater than 0.1%, these equilibria curves show different shapes and be away from their experimental data to some extent. Later, the Modified Quasi chemical Model in the pair approximation in consideration of the strong short-range ordering mainly between Al, Fe and O have been used to establish the thermodynamic equilibrium relationship by Paek et al.²⁵. It can be concluded from the Fig. 5a that there is not a same curve to describe all these experimental data of Al-deoxidation equilibria in liquid iron. Previous studies reported^{29,30} that the atoms of [Al] and [O] could not be independent randomly distributed, but have a strong tendency to form a kind of metastable phase, such as associated compound AlO, Al₂O etc. In addition, Wang et al.^{32–34} suggested that the thermodynamic of Al-deoxidation in liquid iron is closely related with the size of alumina. Xiao et al.^{35–37} reported that the deoxidation thermodynamics of metal in liquid iron have depended on the structures and properties of reaction products. Hence, it can be concluded that there is a close relationship between the thermodynamics of Al-deoxidation reaction in liquid iron and metastable phase, such nano-Al₂O₃.

Wang et al.^{32–34} reported that the deoxidizers aluminum react with dissolved oxygen in molten steel to form various metastable alumina inclusions at first, and then the metastable alumina inclusion transform into stable crystal. However, the Al-deoxidation reaction in Fe–O–Al melt is very difficult to reach the thermodynamic equilibrium between bulk alumina and Fe–O–Al melt because of low supersaturation. Wasai et al.³¹ suggested that the small alumina nuclei are suspended in liquid iron, and this is one reason for the presence of excess oxygen in liquid iron. Later, Wasai et al.⁸ found a series of nano-alumina by hold their Al-deoxidation experiments at 1873 K in alumina crucible. In their experiments, the Al-deoxidized iron was maintained at 1873 K for a certain time (1, 5, 15, 30, 60 min), and the Al-deoxidized iron was solidified at 3 different cooling speed. The minimum diameter of alumina inclusions observed in their work is in the range from a few nm to 10 nm. This result indicates that the Al-deoxidation products are nanoscale alumina even 60 min after Al-deoxidation in the liquid iron.

As the reaction proceeds, the thermodynamic driving force of Al-deoxidation in liquid iron decreased gradually with the decreasing supersaturation ratio³¹. Therefore, it is very difficult for the nano-Al₂O₃ (or nano-FeAl₂O₄) to grow up into the final bulk crystal at the later period of Al-deoxidation. As a result, the nano-Al₂O₃ (or nano-FeAl₂O₄) are not large enough to float upward, and can appear as the structural units in Fe–O–Al melt and may remain as suspending inclusions in the melt for a long time. Therefore, the reaction products of Al-deoxidation in liquid iron may be various nano-Al₂O₃ and nano-FeAl₂O₄ inclusions in many cases.

Based on the Gibbs free energy changes for the formation of different size of Al₂O₃ and FeAl₂O₄ in liquid iron at 1873 K, the thermodynamic curves for the Al-deoxidation in liquid iron can be obtained. As shown in Fig. 5b, the thermodynamic curves for different size of alumina (solid line) and hercynite (dash line) means that the product of Al-deoxidation in liquid iron can be different size of alumina and hercynite. It should be noted that the diameter of FeAl₂O₄ is 1.6 times that of α -Al₂O₃ when they have the same number of aluminum atoms. This is because of the “molecule densities” of FeAl₂O₄ is 1.6 times as that of Al₂O₃ according to the calculation result. It can be seen from Fig. 5b, most of the Al-deoxidation experimental data are covered by the region between the bulk-alumina (or bulk-hercynite) equilibrium curve and the thermodynamic curves of 2 nm alumina (or 3.2 nm hercynite). Such facts indicate that the Al-deoxidation product should not be bulk-crystal but in nanoscale in most of those equilibria experiments. It can be concluded that the Al-deoxidation experiments by various researchers are in different thermodynamic state. These different thermodynamic states in their experiments may lead by the different experimental conditions. In addition, the nano-alumina (or nano-hercynite) thermodynamic curves are close to the bulk-alumina (or bulk-hercynite) equilibrium curve gradually with the increase of size of Al-deoxidation products. It indicates that the Al-deoxidation reaction is gradually close to the equilibrium between bulk alumina (or bulk-hercynite) and liquid iron with the increasing of Al-deoxidation products size during growth process. In other words, the equilibria experiments of various researchers could be in a state away from the final equilibrium between bulk alumina and liquid iron to some extent.

Thermodynamic coexisting point of the formation of Al₂O₃ and FeAl₂O₄ in liquid iron. As shown in Fig. 6a, the intersection points of thermodynamic curves for alumina and corresponding hercynite (hercynite have the same number of aluminum atoms with alumina) are the thermodynamic coexisting points, while the intersection of thermodynamic curves for bulk alumina and bulk hercynite is the equilibrium coexisting point. The products in these points are both alumina and hercynite, and their size increase from right to left.

As known, there are three phases (liquid iron, hercynite and alumina) in Fe–Al–O ternary system, so the freedom degree is zero if this ternary system is under the specified pressure and temperature. Consequently, there is only one equilibrium coexisting point when the liquid iron equilibrated with both alumina and hercynite. Such an equilibrium coexisting point at 1873 K has been measured by several researchers^{11–13,23,31,47,48}. McLean et al.¹¹ measured the oxygen content of liquid iron in equilibrium with Al₂O₃ and FeO·Al₂O₃ at temperatures between 1823 and 2023 K, and reported the coexisting point to be 6.23×10^{-2} [% O], 1.4×10^{-5} [% Al] at 1873 K. Kim et al.⁴⁷ measured the equilibrium at the temperature between 1813 and 1983 K, and reported the coexisting point to be 7.4×10^{-2} [% O], 1.1×10^{-5} [% Al] at 1873 K. Hilty et al.¹² reported the coexisting point (8×10^{-2} [% O], 2×10^{-3} [% Al]) by melting oxidized electrolytic Fe in alumina crucible or adding FeO to Fe–Al melt at 1873 K. Meanwhile, Wasai and Mukai³¹ reported their coexisting point to be 7.4×10^{-2} [% O], 6.3×10^{-3} [% Al] using an associated solution model at 1873 K. It should be noticed that the oxygen concentrations of coexisting point are close to each other, but the difference about the aluminum concentrations is more than two orders magnitude in these experiments, as shows in the Fig. 6b.

These equilibria experiments may be in the different thermodynamic states due to different experimental conditions. Thus, the deoxidation products maybe a series of different size nanoscale hercynite and alumina in their three-phase equilibrium experiments. These different values of equilibrium coexisting points by various researchers may have a close relationship with the size of Al-deoxidation products. In some case of experiments, the three equilibrium coexisting phases in Fe–O–Al melt could be nano-alumina, nano-hercynite and liquid

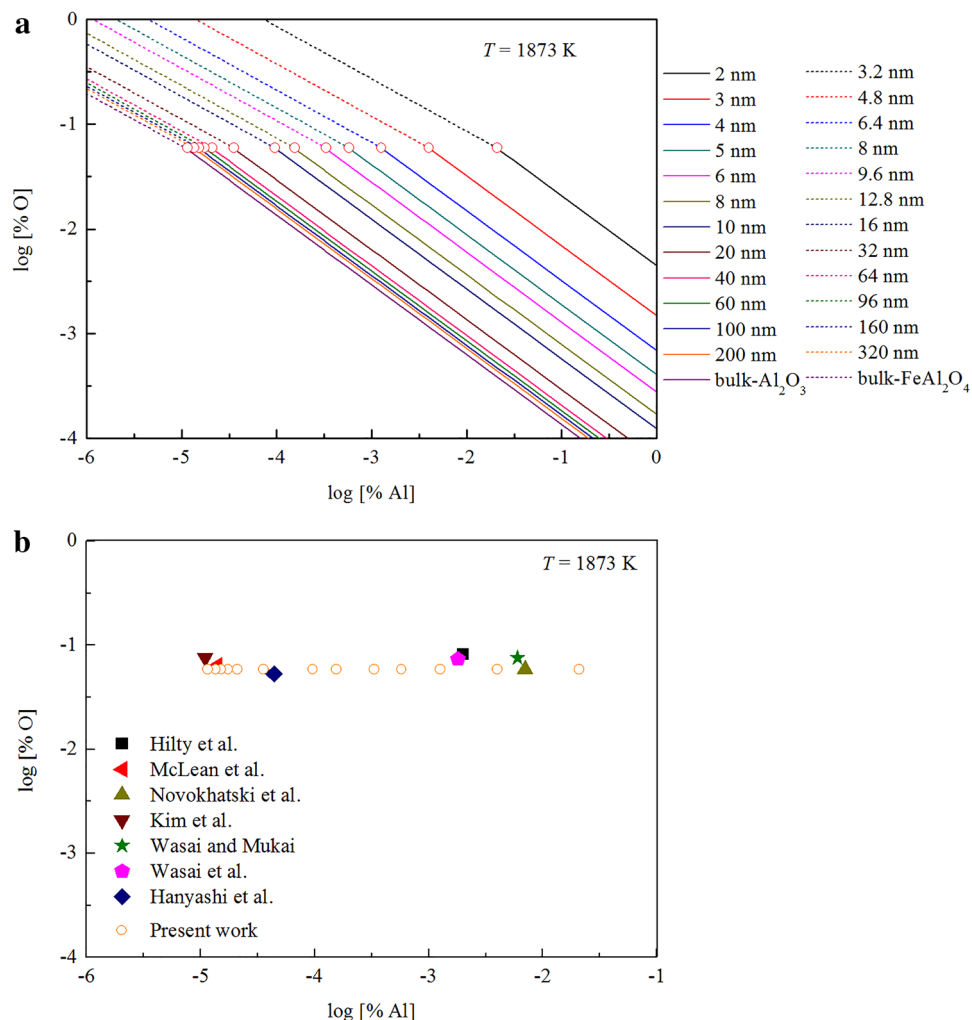


Figure 6. Thermodynamic coexisting points for the formation of Al_2O_3 and FeAl_2O_4 in liquid iron at 1873 K. (a) The thermodynamic coexisting points obtained by this work, (b) comparison between the present thermodynamic coexisting points and previous equilibrium coexisting point.

iron. Therefore, the coexisting points may be different to each other. As can be seen from Fig. 6b, all the predicted coexisting points are located at the same horizontal line. The concentrate of [Al] at the coexisting point for 2 nm Al_2O_3 is more than three orders of magnitude less than that for bulk Al_2O_3 . These results agree well with the previous experimental data^{11–13,23,31,47,48}. Such a fact indicates that it needs more time for the nano- Al_2O_3 (or nano- FeAl_2O_4) to grow up into bulk- Al_2O_3 (or bulk- FeAl_2O_4) in some cases. It suggested that these coexisting points measured by various experiments could be in different thermodynamic state. Most of the products of three-phase equilibrium in Fe–O–Al melt are not bulk- Al_2O_3 and bulk- FeAl_2O_4 but also various different size nano- Al_2O_3 and nano- FeAl_2O_4 . Thus, these coexisting points proved again that many previous experiments are close to the final equilibrium, but not reach the final equilibrium.

Conclusions

The conclusions are as follows:

- (1) The surface of nano-alumina or nano-hercynite plays an important part in their thermodynamic properties. The Gibbs free energy changes for the formation of nano- Al_2O_3 and nano- FeAl_2O_4 decrease with the increasing size and increase with the increasing temperature. The Gibbs free energy changes for transformation of nano- Al_2O_3 into bulk- Al_2O_3 increase with the increasing size and temperature.
- (2) The published experimental data for Al-deoxidation equilibria in liquid iron are scattered across the region between the thermodynamic curve of nano-alumina (or nano-hercynite) and the equilibrium curve of bulk-alumina (or bulk-hercynite). The thermodynamic coexisting points about Al_2O_3 and FeAl_2O_4 in liquid iron are in a straight line and coincide with the various previous data.

- (3) Many of the previous Al-deoxidation experiments are close to the final thermodynamic equilibrium between bulk alumina or hercynite and liquid iron but not reach the final thermodynamic equilibrium because their partial product is nano-alumina or nano-hercynite.

Received: 5 June 2020; Accepted: 15 September 2020

Published online: 09 October 2020

References

- Tuttle, R. B., Smith, J. D. & Peaslee, K. D. Interaction of alumina inclusions in steel with calcium-containing materials. *Metall. Mater. Trans. B* **36**, 885–892 (2005).
- Tabatabaei, Y., Coley, K. S., Irons, G. A. & Sun, S. A multilayer model for alumina inclusion transformation by calcium in the ladle furnace. *Metall. Mater. Trans. B* **49**, 375–387 (2018).
- Goto, H., Miyazawa, K. & Kadoya, T. Effect of the composition of oxide on the reaction between oxide and sulfur during solidification of steels. *ISIJ Int.* **35**, 1477–1482 (1995).
- Oikawa, K., Ishida, K. & Nishizawa, T. Effect of titanium addition on the formation and distribution of MnS inclusions in steel during solidification. *ISIJ Int.* **37**, 332–338 (1997).
- Byun, J. S., Shim, J. H., Cho, Y. W. & Lee, D. N. Non-metallic inclusion and intragranular nucleation of ferrite in Ti-killed C-Mn steel. *Acta Mater.* **51**, 1593–1606 (2003).
- Liu, Z., Kobayashi, Y., Yin, F., Kuwabara, M. & Nagai, K. Nucleation of acicular ferrite on sulfide inclusion during rapid solidification of low carbon steel. *ISIJ Int.* **47**, 1781–1788 (2007).
- Zhao, Y. *et al.* Mechanisms on superfine alumina inclusions formation by Al-deoxidation reaction for liquid iron. *Steel Res.* **89**, 1800255 (2018).
- Wasai, K., Mukai, K. & Miyanaga, A. Observation of inclusion in aluminum deoxidized iron. *ISIJ Int.* **42**, 459–466 (2002).
- Yang, W., Duan, H., Zhang, L. & Ren, Y. Nucleation, growth, and aggregation of alumina inclusions in steel. *JOM* **65**, 1173–1180 (2013).
- The 19th Committee in Steelmaking, Thermodynamic Data For Steelmaking, The Japan Society for Promotion of Science*, 10. Tohoku University Press, Sendai, Japan (2010).
- McLean, A. & Ward, R. G. Thermodynamics of hercynite formation. *J. Iron Steel Inst.* **204**, 8–11 (1966).
- Hilty, D. C. & Crafts, W. The solubility of oxygen in liquid iron containing aluminum. *JOM* **2**, 414–424 (1950).
- Novokhatskiy, I. A. & Belov, B. F. Phase equilibria and distribution of elements in the Fe–O–Al system. *Russ. Metall.* **1**, 12–14 (1966).
- Schenck, H., Steinmetz, E. & Mehta, K. K. Equilibrium and kinetics of precipitation of alumina in system iron-oxygen-aluminium at 1600 °C. *Arch. Eisenhüttenwes.* **41**, 131–138 (1970).
- Fruehan, R. Activities in liquid Fe–Al–O and Fe–Ti–O alloys. *Metall. Trans.* **1**, 3403–3410 (1970).
- Rohde, L., Choudhury, A. & Wahlster, M. New investigation into the aluminium–oxygen equilibrium in iron melt. *Arch. Eisenhüttenwes.* **42**, 165–174 (1971).
- Janke, D. & Fischer, W. Deoxidation equilibria of Ti, Al and Zr in Fe melts at 1600 °C. *Arch. Eisenhüttenwes.* **47**, 195–198 (1976).
- Shevtsov, V. E. Thermodynamics of oxygen solutions in the Fe–Al System. *Russ. Metall.* **1**, 52–57 (1981).
- Suito, H., Inoue, H. & Inoue, R. Aluminium–oxygen equilibrium between CaO–Al₂O₃ melts and liquid iron. *ISIJ Int.* **31**, 1381–1388 (1991).
- Suito, H., Inoue, R. & Nagatani, A. Mullite as an electrochemical probe for the determination of low oxygen activity in liquid iron. *Steel Res.* **63**, 419–425 (1992).
- Dimitrov, S., Weyl, A. & Janke, D. Control of the manganese–oxygen reaction in pure iron melts. *Steel Res.* **66**, 87–92 (1995).
- Seo, J. D., Kim, S. H. & Lee, K. R. Thermodynamic assessment of the Al deoxidation reaction in liquid iron. *Steel Res.* **69**, 49–53 (1998).
- Hayashi, A., Uenishi, T., Kandori, H., Miki, T. & Hino, M. Aluminum deoxidation equilibrium of molten Fe–Ni alloy coexisting with alumina or hercynite. *ISIJ Int.* **48**, 1533–1541 (2008).
- Kang, Y. *et al.* Aluminum deoxidation equilibrium of molten iron–aluminum alloy with wide aluminum composition range at 1873 K. *ISIJ Int.* **49**, 1483–1489 (2009).
- Paek, M. K., Jang, J. M., Kang, Y. B. & Pak, J. J. Aluminum deoxidation equilibria in liquid iron: Part I. Experimental. *Metall. Mater. Trans. B* **46**, 1826–1836 (2015).
- Cho, S. & Suito, H. Assessment of aluminum–oxygen equilibrium in liquid iron and activities in CaO–Al₂O₃–SiO₂ slags. *ISIJ Int.* **34**, 177–185 (1994).
- Sigworth, G. & Elliott, J. The thermodynamics of liquid dilute iron alloys. *Metal Sci.* **8**, 298–310 (1974).
- Itoh, H., Hino, M. & Ban-Ya, S. Thermodynamics on the formation of spinel nonmetallic inclusion in liquid steel. *Mater. Trans. B* **28**, 953–956 (1997).
- Wasai, K. & Mukai, K. Thermodynamic analysis of Fe–Al–O liquid alloy equilibrated with alpha-Al₂O₃(s) by an associated solution model. *J. Jpn. Inst. Met.* **52**, 1088–1097 (1988).
- Jung, I. H., Deckerov, S. A. & Pelton, A. D. A thermodynamic model for deoxidation equilibria in steel. *Metall. Mater. Trans. B* **35**, 493–507 (2004).
- Wasai, K. & Mukai, K. Thermodynamics of nucleation and supersaturation for the aluminum–deoxidation reaction in liquid iron. *Metall. Mater. Trans. B* **49**, 1065–1074 (1999).
- Wang, G. C., Wang, Q., Li, S., Ai, X. & Li, D. A multi-step thermodynamic model for alumina formation during aluminum deoxidation in Fe–O–Al melt. *Acta Metall. Sin.* **28**, 272–280 (2015).
- Wang, G., Xiao, Y., Zhao, C., Li, J. & Shang, D. Atomic cluster aggregates in nucleation of solid alumina inclusion in the aluminum deoxidation for liquid iron. *Metall. Mater. Trans. B* **49**, 282–290 (2018).
- Wang, G., Wang, Q., Li, S., Ai, X. & Fan, C. Evidence of multi-step nucleation leading to various crystallization pathways from an Fe–O–Al melt. *Sci. Rep.* **4**, 5082 (2014).
- Xiao, Y. *et al.* Nucleation and growth for magnesia inclusion in Fe–O–Mg melt. *RSC Adv.* **8**, 38336–38345 (2018).
- Xiao, Y. *et al.* Thermodynamic modelling on nanoscale growth of magnesia inclusion in Fe–O–Mg melt. *Metals* **9**, 174 (2019).
- Xiao, Y. *et al.* Thermodynamic insight into the growth of calcia inclusions at the nanoscale: The case of Fe–O–Ca melt. *RSC Adv.* **9**, 11135–11141 (2019).
- Meng, Q., Zhou, N., Rong, Y., Chen, S. & Hsu, T. Y. Size effect on the Fe nanocrystalline phase transformation. *Acta Mater.* **50**, 4563–4570 (2002).
- Zu, X., Birringer, R., Herr, U. & Gleiter, H. X-ray diffraction studies of the structure of nanometer-sized crystalline materials. *Phys. Rev. B* **35**, 9085 (1987).
- Sui, M. L. *et al.* Positron-lifetime study of polycrystalline Ni–P alloys with ultrafine grains. *Phys. Rev. B* **44**, 6466 (1991).

41. Herr, U. Metastable phases in interface controlled materials. *Contemp. Phys.* **41**, 93–104 (2000).
42. Dash, J. G. Surface melting. *Contemp. Phys.* **30**, 89–100 (1989).
43. Thomas, G. J. & Siegel, R. W. Grain boundaries in nanophase palladium: High resolution electron microscopy and image simulation. *Scr. Metall.* **24**, 201–206 (1990).
44. Phillpot, S. R., Wolf, D. & Gleiter, H. Molecular dynamics study of the synthesis and characterization of a fully dense, three-dimensional nanocrystalline material. *J. Appl. Phys.* **78**, 847–861 (1995).
45. Waniewska, A. S. & Greneche, J. M. Magnetic interfaces in Fe-based nanocrystalline alloys determined by Mössbauer spectrometry. *Phys. Rev. B* **56**, 8491 (1997).
46. Perdew, J. P., Burke, K. & Ernzerhof, M. Generalized gradient approximation made simple. *Phys. Rev. Lett.* **77**, 3865 (1996).
47. Kim, C. K., McLean, A. *Metal-Slag-Gas Reactions and Processes, the Electrochemical Society Conference, Toronto, Canada*, 284–295 (1975).
48. Wasai, K., Mukai, K., Fuchiwaki, H. & Yoshida, A. Determination of aluminum and oxygen contents in liquid iron in equilibrium with α -alumina and hercynite. *ISIJ Int.* **39**, 760–766 (1999).

Acknowledgements

We acknowledge the funding support from National Natural Science Foundation of China and Shanghai Baosteel (Grant No. U1460108), National Natural Science Foundation of China (Grant Nos. 51874170, 51604253, 51634004 and 51574074).

Author contributions

H.L. and G.W. designed research. Y.X. performed research. H.Z., W.J. and L.Z. analyzed data, and Y.X. wrote the paper.

Competing interests

The authors declare no competing interests.

Additional information

Correspondence and requests for materials should be addressed to G.W.

Reprints and permissions information is available at www.nature.com/reprints.

Publisher's note Springer Nature remains neutral with regard to jurisdictional claims in published maps and institutional affiliations.



Open Access This article is licensed under a Creative Commons Attribution 4.0 International License, which permits use, sharing, adaptation, distribution and reproduction in any medium or format, as long as you give appropriate credit to the original author(s) and the source, provide a link to the Creative Commons licence, and indicate if changes were made. The images or other third party material in this article are included in the article's Creative Commons licence, unless indicated otherwise in a credit line to the material. If material is not included in the article's Creative Commons licence and your intended use is not permitted by statutory regulation or exceeds the permitted use, you will need to obtain permission directly from the copyright holder. To view a copy of this licence, visit <http://creativecommons.org/licenses/by/4.0/>.

© The Author(s) 2020